J. Fluid Mech. (1995), *vol.* 302, *pp.* 231–257

The effect of surfactant on bursting gas bubbles

By JEREMY M. BOULTON-STONE

School of Mathematics and Statistics,
The University of Birmingham, Edgbaston, Birmingham B15 2TT, UK

(Received 31 January 1995 and in revised form 29 June 1995)

A numerical technique, based on the boundary integral method, is developed to allow the modelling of unsteady free-surface flows at large Reynolds numbers in cases where the surface is contaminated by some surface-active compound. This requires the method to take account of the tangential stress condition at the interface and is achieved through a boundary-layer analysis. The constitutive relation that forms the surface stress condition is assumed to be of the Boussinesq type and allows the incorporation of surface shear and dilatational viscous forces as well as Marangoni effects due to gradients in surface tension. Sorption kinetics can be included in the model, allowing calculations for both soluble and insoluble surfactants. Application of the numerical model to the problem of bursting gas bubbles at a free surface shows the greatest effect to be due to surface dilatational viscosity which drastically reduces the amount of surface compression and can slow and even prevent the formation of a liquid jet. Surface tension gradients give dilatational elasticity to the surface and thus also significantly prevent surface compression. Surface shear viscosity has a smaller effect on the interface motion but results in initially increased surface concentrations due to the sweeping up of surface particles ahead of the inward-moving surface wave.

1. Introduction

The ability to model in a realistic manner physically occurring free-surface flows has many important engineering and biological applications. The boundary integral method used to model free-surface flows at high Reynolds numbers (Guerri, Lucca & Prosperetti 1981) provides an efficient, yet highly accurate technique in cases where the tangential stress component at the surface is small, for example at pure interfaces. However where surfactants are adsorbed onto the surface, this is not necessarily the case. Gradients in surface tension and surface viscous effects can give rise to large tangential stresses at interfaces. It would therefore be beneficial to be able to modify the boundary integral method to allow for the inclusion of more realistic surface properties.

In this paper, we develop an extension to the boundary integral method which allows the specification of a tangential stress condition at large Reynolds numbers. We apply this to the problem of a gas bubble bursting at a contaminated free surface. The results are compared to those of Boulton-Stone & Blake (1993, hereinafter referred to as BSB), where a pure liquid was assumed.

Several studies, both analytical and numerical, of the effects of surfactants have been concerned with the fundamental problem of calculating the flow field around a rising gas bubble for the case where surface tension is a function of the surface

concentration of surfactant (Levich 1962; Harper 1972). Indeed for dilute solutions with a small Weber number (so that the bubble can be assumed spherical), the increase in the drag coefficient due to the compression of surfactant at the rear of the bubble is now well understood for both large and small Reynolds numbers, and high and low surface activity (Harper 1974, 1988). For more concentrated surfactant solutions, the flow field itself must be found as part of the solution, thus rendering the problem nonlinear. Nevertheless, the observation by Savic (1953) of a stagnant region at the rear of the bubble surface in some cases allows theoretical calculation of the drag coefficients (Harper 1973). This case has been solved exactly, in terms of an infinite series of associated Legendre functions, by Sadhal & Johnson (1983).

The effect of surface viscosity in steady bubble rise problems is unlikely to be of much interest since it is probably only going to be important at sufficiently large surface concentrations which render the surface immobile. However for unsteady problems of the kind studied numerically using techniques such as the boundary integral method, surface viscous forces can play a critical role in the determination of the surface and surrounding fluid motion. Simple unsteady problems such as the effect of surfactants on small-amplitude plane waves can be dealt with analytically. Many studies reported in the literature (Lucassen & van den Tempel 1972; Avramidis & Jiang 1991; Lemaire & Langevin 1992; Johnson & Stebe 1994) relate theoretical models of unsteady flows to techniques for measuring surface viscous properties. In the bursting bubbles situation (see also BSB), used here as a case study, there is very strong surface compression during the moments immediately prior to the formation of the liquid jet. This surface compression can be seen by examining the significant calculated increase in the surface concentration of a passive surfactant in the otherwise pure liquid case (see §6). We therefore anticipate, and later verify, this surface concentration increase (as well as the large energy dissipation rates calculated by both BSB and Garcia-Briones & Chalmers 1993) as the jet forms, to be inhibited by a surface dilatational viscosity. In addition, surface dilatational viscosity may prevent or suppress jet formation.

Boundary-layer approximations for the case of a stress-free interface have been used previously together with boundary integral methods. Using such techniques, Lundgren & Mansour (1988) were able to find the first-order correction to the normal velocity for large Reynolds numbers. This work was extended by BSB to enable the calculation of the tangential velocity perturbation. For most applications, including bursting and collapsing bubbles, the effect of these perturbations is only slight since the normal and tangential velocity perturbations are $O(Re^{-1})$ and $O(Re^{-1/2})$ respectively for large Reynolds number, Re. However, an effect is apparent for periodic motions over many oscillations, as in the case of the Lundgren & Mansour (1988) study of oscillating drops.

If surfactants are present on a bubble's surface it is no longer appropriate to assume that the tangential component of stress is zero. It is also erroneous to assume that the purely inviscid boundary integral method will necessarily give an accurate estimate of the true motion as in the case of a pure interface. In order to make progress, some form of boundary-layer analysis should be considered if we wish to use a boundary integral technique to solve a problem involving surfactant solutions. In the case where the surface stress terms due to the presence of the surfactant are much larger than the bulk viscous stresses at the interface, the method of Nadim, Kumar & Greenspan (1993), in which the tangential velocity is found through a balance of the tangential component of surface stresses either side of the interface, can be used.

In this paper we describe (see §§4 and 5) a numerical technique based on the Boussinesq surface model. This allows us to take into account variations in surface tension (due to variations in surfactant concentration at the surface) giving rise to Marangoni effects, and surface viscous forces (shear and dilatational) which introduce a certain amount of rigidity to the surface. The method will handle both soluble and insoluble surfactants. To show the general applicability of the numerical method, we include a number of parameters in the following theoretical development. However in most practical situations we are going to be interested in only a few of the physical processes described by these parameters.

Denoting all dimensional quantities by a superscript asterisk, the bulk diffusion coefficient, D^*, for the surfactant is almost invariably smaller than the kinematic viscosity, ν^*, so for a problem with large Reynolds number, $2U^*a^*/\nu^*$ (U^* and a^* being the velocity scale and bubble radius respectively), the corresponding Péclet number, $2U^*a^*/D^*$, will also be large. This means that there will exist a concentration boundary layer where the concentration adjusts from a uniform concentration away from the surface to some value near to the surface sublayer.

In transporting surfactant from the bulk to the surface, there are two competing physical processes in operation. One is the diffusion from the bulk to the liquid near to the surface (i.e. to the sublayer within the boundary layer), the other is the adsorption to, and desorption from, the surface itself. If these two processes take place over differing timescales, the slowest of them will limit the rate of transport. In this case, the Péclet number is large so that diffusion is slow compared with the bubble burst.

There is one special limiting case for the sorption rate. If the surfactant can be considered insoluble, i.e. adsorption is much faster than desorption, or both desorption and adsorption take place over a much longer timescale than the bubble burst, we may assume that the flux term in the equation for the transport of adsorbed surfactant will be zero. In this case, the surface concentration is effectively decoupled from the bulk concentration so that there is no need to find the bulk concentration as part of the solution. Otherwise we need to consider advection and diffusion of the dissolved surfactant in order to identify the flux from the liquid phase to the gas/liquid interface.

The details of the derivation and implementation of the method used to incorporate surface viscous and Marangoni effects are described, in the context of the bubble bursting problem, in the following sections (§§2–5). A discussion of the effects of some of the parameters and surface properties on the bursting of a gas bubble can be found in §6.

2. Formulation

2.1. *Surfactant kinetics and dynamics*

Immediately before our calculations begin, we assume that the bubble rests in an equilibrium position where the upward buoyant force balances the downward force due to the surface tension in the film separating the bubble from the atmosphere above. As in BSB, we ignore the rupture of the film itself which takes place over a much smaller timescale than the subsequent motion of the bubble, the subject of our interest here. We start our calculations at time $t^* = 0$ with the assumption that the film has completely ruptured, leaving a crater in the surface of the fluid, which then collapses under the influence of surface tension and gravity.

Since the bubble typically rests for some time before the film above the bubble thins to its critical thickness and ruptures (maybe of the order of seconds or longer depending on the surfactant properties), we make the assumption that the bulk and surface concentrations are initially in equilibrium (sorption processes take place on the order of 10^{-2} s (Lin, McKeigue & Maldarelli 1991)). Further we assume, for the purposes of these calculations, that diffusion in the bulk and the surface will ensure that the initial bulk and surface concentrations are constants, C_0^* and Γ_0^* respectively. Initially, the fluid itself is taken to be at rest.

In the model, sorption processes are governed by Langmuir kinetics so that the net flux to the surface is of the form

$$j_n^* = -P^*(\Gamma^*) + Q^*(\Gamma^*, C^*|_0), \tag{2.1}$$

where Γ^* and C^* are the surface and bulk concentrations, and $|_0$ denotes evaluation at the interface. For $0 \leqslant \Gamma^* \leqslant \Gamma_\infty^*$, the desorptive and adsorptive fluxes, P^* and Q^*, are given by

$$P^*(\Gamma^*) = k_2^* \Gamma^* \quad \text{and} \quad Q^*(\Gamma^*, C^*|_0) = k_1^* C^*|_0 \left(1 - \frac{\Gamma^*}{\Gamma_\infty^*}\right), \tag{2.2}$$

where Γ_∞^* is taken to be the maximum packing density for adsorbed surfactant, and k_1 and k_2 are adsorptive and desorptive rate constants, respectively.

At equilibrium, $j_n^* = 0$ and so Γ_0^* (the surface concentration in equilibrium with C_0^*, which for $t^* > 0$ is also the bulk concentration at infinity) is given by the expression

$$\Gamma_0^* = \frac{(k_1^*/k_2^*) C_0^* \Gamma_\infty^*}{\Gamma_\infty^* + (k_1^*/k_2^*) C_0^*}. \tag{2.3}$$

The surface tension, σ^*, is given by a surface equation of state, which we write in the form (Jensen & Grotberg 1992)

$$\sigma^* = \sigma_\infty^* + (\sigma_p^* - \sigma_\infty^*)\sigma_1(\Gamma^*/\Gamma_\infty^*), \quad 0 \leqslant \Gamma^* \leqslant \Gamma_\infty^*, \tag{2.4}$$

where σ_p^* is the surface tension of the pure liquid, σ_∞^* is the value when the surface is saturated, i.e. when $\Gamma^* = \Gamma_\infty^*$, and σ_1 is a function satisfying $\sigma(0) = 1$ and $\sigma(1) = 0$. For a bubble bursting in a pure liquid, preliminary calculations indicate that the surface fluid is compressed strongly as a result of the flow converging towards the axis of symmetry. We therefore expect surface surfactant concentrations to increase markedly for contaminated bubbles, and it seems likely that a nonlinear surface equation of state should be used. The precise form for σ_1 depends strongly on the type of surfactant present, but here we assume the form given in Gaver & Grotberg (1990),

$$\sigma_1(x) = (\alpha + 1)(1 + \theta(\alpha)x)^{-3} - \alpha, \tag{2.5}$$

where $\theta(\alpha) = (1 + 1/\alpha)^{1/3} - 1$. The parameter α governs the nonlinearity of the equation of state: as α becomes small, $\sigma^* \to \sigma_\infty^*$ for all $\Gamma^* > 0$; as α becomes large, $\sigma_1(x) \to 1 - x$.

In order to describe the motion of the adsorbed surfactant, we employ a convection–diffusion equation for the surface concentration of surfactant, upon which the surface viscosities and surface tension depend. Mass conservation incorporating the flux from the bulk phase, j_n^*, implies that this equation must be of the form

$$\frac{\mathrm{D}\Gamma^*}{\mathrm{D}t^*} + \Gamma^* \nabla_s^* \cdot \boldsymbol{v}^* = D_s^* \nabla_s^{*2} \Gamma^* + j_n^*, \tag{2.6}$$

where the symbol ∇_s^* is used to denote the surface gradient operator, and $\boldsymbol{v}^*$ is the fluid velocity. The corresponding equation for the evolution of the bulk concentration is

$$\frac{DC^*}{Dt^*} = D^*\nabla^{*2}C^*. \tag{2.7}$$

We assume that the stress jump at the interface is determined by a linear Boussinesq scheme (Slattery 1990). In this model, the stress tensor is written as the sum of the usual Newtonian bulk-phase stress tensor and the divergence of a surface stress tensor, linear in the surface velocity, which allows for surface viscous effects as well as the more familiar normal and tangential stresses due to surface tension. The two viscous parameters are the surface shear and surface dilatational viscosities, μ_s^* and κ_s^* respectively. The surface shear viscosity is defined analogously to bulk shear viscosity; the dilatational viscosity can be thought of as the coefficient of an additional surface tension proportional to the fractional rate of change of the surface area, i.e. $\Delta\sigma^* = \kappa_s^*(1/A^*)(dA^*/dt^*)$ (Adamson 1982) where A^* is the surface area.

The surface stress tensor is defined as (Slattery 1990)

$$\boldsymbol{S}_s^* = 2\mu_s^*\boldsymbol{E}_s^* + (\kappa_s^* - \mu_s^*)\boldsymbol{D}_s^* + \sigma^*\boldsymbol{I}_s, \tag{2.8}$$

where $\boldsymbol{I}_s = \boldsymbol{I} - \hat{\boldsymbol{n}}\hat{\boldsymbol{n}}$ is the surface identity, with $\hat{\boldsymbol{n}}$ the outward-pointing normal to the interface, as shown in figure 1, and where

$$\boldsymbol{D}_s^* = \boldsymbol{I}_s\nabla_s^*\cdot\boldsymbol{v}^* \quad \text{and} \quad \boldsymbol{E}_s^* = \tfrac{1}{2}\{(\nabla_s^*\boldsymbol{v}^*)\cdot\boldsymbol{I}_s + \boldsymbol{I}_s\cdot(\nabla_s^*\boldsymbol{v}^*)^T\}. \tag{2.9}$$

For axisymmetric flow, $(\nabla_s^*\boldsymbol{v}^*)\cdot\boldsymbol{I}_s$ is symmetric so that we can write $\boldsymbol{E}_s^* = (\nabla_s^*\boldsymbol{v}^*)\cdot\boldsymbol{I}_s$.

2.2. *Non-dimensionalization*

The lengthscale for the problem is the equivalent radius of the bubble defined as $a^* = (3V^*/4\pi)^{1/3}$ where V^* is the bubble volume prior to film rupture. We assume a general timescale, T^*, and an associated velocity scale, U^*, given by $U^* = a^*/T^*$, with pressures scaling as ρ^*U^{*2} where ρ^* is the liquid density.

As indicated above, values for the surface tension and the surface viscosities will be concentration dependent. The surface tension is scaled with respect to the surface tension of the pure liquid, σ_p^*, whereas the surface viscosities (assumed zero for the pure liquid) are scaled with respect to the initial, equilibrium, values and are thus indicated by a subscript 0.

In addition to the functional dependencies of the surface parameters on surface concentration, there are six independent, non-dimensional parameters to this problem. In order to define the fluid bulk properties the Morton number, $M = g\rho^{*3}\nu^{*4}/\sigma_p^{*3}$ where g is the gravitational acceleration, is used. The bubble size is chosen via the Eötvös number, $Eo = (2a^*)^2\rho^*g/\sigma_p^*$. The surface viscosities can be written in terms of the two parameters $\beta_s = \mu_{s0}^*/2a^*\mu^*$ and $\beta_d = \kappa_{s0}^*/2a^*\mu^*$, where $\mu^* = \rho^*\nu^*$ is the dynamic viscosity.

The fifth and sixth parameters are Schmidt numbers, determining the amount of bulk and surface diffusion as ratios of the bulk viscosity to the respective diffusion coefficients: $Sc = \mu^*/D^*\rho^*$ and $Sc_s = \mu^*/D_s^*\rho^*$. The form of the equations is clearer if written in terms of the Reynolds and Péclet numbers: in terms of the above parameters, the Reynolds number is given by $Re = 2a^*\rho^*U^*/\mu^* = (We^2Eo/M)^{1/4}$; and the bulk and surface Péclet numbers by $Pe = 2a^*U^*/D^* = ReSc$ and $Pe_s = 2a^*U^*/D_s^*ReSc_s$.

The Weber number, $We = 2a^*\rho^*U^{*2}/\sigma_p^*$, also appears in the equations of motion, but disappears once we decide upon a natural timescale due to the collapse of

a bursting bubble under the influence of surface tension (as we do here), $T^* = (\rho^* a^{*3}/\sigma_p^*)^{1/2}$, or for example to the acceleration of a bubble rising under the influence of gravity, $T^* = (a^*/g)^{1/2}$, in which cases the Weber number becomes 2 or $Eo/2$ respectively. In cases where the velocity scale, U^*, is itself a parameter of the problem, it may be more convenient to express the gravitational body force in terms of a Froude number, $Fr = U^{*2}/2a^*g$, rather than as a ratio of Eötvös and Weber numbers.

We scale bulk and surface concentrations with respect to C_0^* and Γ_0^* respectively. This leads to the dimensionless flux being expressible as

$$j_n = K\left\{C|_0\left(\frac{\Gamma_\infty - \Gamma}{\Gamma_\infty - 1}\right) - \Gamma\right\}, \tag{2.10}$$

where $K = k_2^* T^*$ so that K^{-1} represents the dimensionless desorption timescale, and $\Gamma_\infty = 1 + \Gamma_\infty^*/(C_0^* k_1^*/k_2^*)$. The quantity j_n must, in addition, be equal to the diffusional flux from the bulk, so that we also have

$$j_n = -\frac{2}{hPe}\frac{\Gamma_\infty}{\Gamma_\infty - 1}\frac{\partial C}{\partial n}, \tag{2.11}$$

where h is defined as $h = k_1^*/a^* k_2^*$. If $\Gamma_\infty^* \gg (k_1^*/k_2^*)C_0^*$ then, from (2.3), $ha^* \sim (\Gamma_0^*/C_0^*)$ so that h may be viewed as a non-dimensional adsorption depth. Also h^{-1} is a measure of the solubility of the surfactant (Jensen & Grotberg 1993). However, boundary-layer theory (see below also) indicates that the order of magnitude of the $\partial C/\partial n$ term in (2.11) is $Pe^{1/2}$ times the difference in the values of the bulk concentration at the boundary and outside the boundary layer. This suggests that the size of the flux, j_n, is proportional to k^{-1}, where k is the activity of the surfactant (Harper 1974), defined as $k = h/\delta_c$, and $\delta_c = Pe^{-1/2}$ is the non-dimensional concentration boundary-layer thickness. We therefore assume that we can ignore the flux term, thus decoupling the bulk concentration from the calculation, when $k \gg 1$. In cases where the surfactant is considered to be soluble, (2.10) and (2.11) provide a boundary condition for the bulk concentration, coupling it to the surface concentration.

In terms of non-dimensional quantities, the equation of state, (2.4), becomes

$$\sigma = \sigma_\infty + (1 - \sigma_\infty)\sigma_1(\Gamma/\Gamma_\infty). \tag{2.12}$$

The deviations of the surface viscosities from their equilibrium values are represented by the coefficients μ_s and κ_s so that, for instance, $\mu_s = 1$ when $\Gamma = 1$, corresponding to the dimensional values of μ_{s0}^* and Γ_0^* respectively. In the calculations presented here, we assume (for a lack of any definite theory) that the dependence of surface viscosities upon surface concentrations is linear, so that $\mu_s = \kappa_s = \Gamma$. The obvious alternative is to keep the surface viscosities constant, i.e. $\mu_s = \kappa_s = 1$. However, this gives results that are graphically indistinguishable over much of the early motion, since high surface concentrations only occur as the liquid jet forms (see §6), from which time results differ only by a few percent. This being the case, the former choice, where surface viscosities are small when surface concentrations are small, seems more reasonable.

Consideration of the sorption kinetics and the equation of state gives five additional dimensionless parameters: K, h, Γ_∞, σ_∞ and α; a total of 11, with the six mentioned above.

2.3. *Evaluation of boundary conditions*

For a pure system, the stress balance at a surface expresses the equality of the bulk stress in the liquid with the normal stress due to the pressure in the gas phase. In

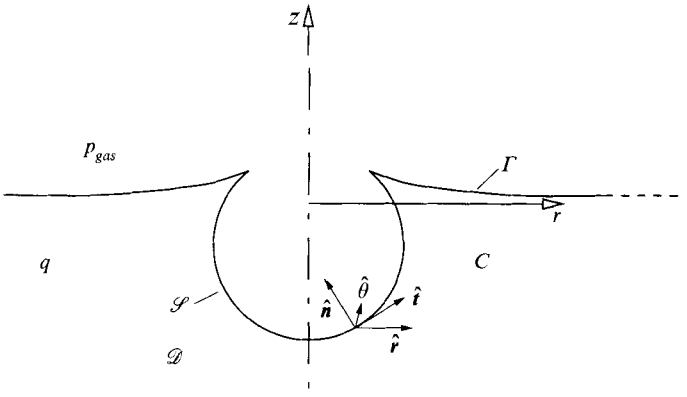

FIGURE 1. Schematic showing the geometry of the bursting bubble problem. Some notation is marked on the diagram: the pressure p_{gas} in the atmosphere, q in the liquid; $\mathscr{S}$, the interface; $\mathscr{D}$, the liquid; the surface and bulk concentrations Γ and C. Also shown are the surface-fitted coordinate system, which is based upon normal, tangential and azimuthal unit vectors, $\{\hat{\boldsymbol{n}}, \hat{\boldsymbol{t}}, \hat{\boldsymbol{\theta}}\}$, and the radial unit vector, $\hat{\boldsymbol{r}}$, of a cylindrical polar coordinate system, (r, z, θ).

order to handle contaminated interfaces (as mentioned in §1) a surface stress term needs to be added. For normals pointing towards the gaseous phase, this condition takes the form

$$-p_{gas}\hat{\boldsymbol{n}} = \hat{\boldsymbol{n}}\cdot\boldsymbol{S} - \nabla_s\cdot\boldsymbol{S}_s, \tag{2.13}$$

where p_{gas} is the pressure on the gaseous side of the interface and $\boldsymbol{S}$ is the bulk stress tensor given by $\boldsymbol{S} = -q\boldsymbol{I} + 4Re^{-1}\boldsymbol{E}$, q being the liquid pressure and $\boldsymbol{E} = \frac{1}{2}\{\nabla\boldsymbol{v} + (\nabla\boldsymbol{v})^T\}$. In terms of dimensionless quantities, the Boussinesq surface stress tensor, given by (2.8), is

$$\boldsymbol{S}_s = 4Re^{-1}\left(2\beta_s\mu_s\boldsymbol{E}_s + (\beta_d\kappa_s - \beta_s\mu_s)\boldsymbol{D}_s\right) + 2We^{-1}\sigma\boldsymbol{I}_s, \tag{2.14}$$

with $\boldsymbol{D}_s$ and $\boldsymbol{E}_s$ corresponding to their dimensional counterparts defined by (2.9).

We now introduce an orthogonal, surface-fitted coordinate system, $\{\hat{\boldsymbol{n}}, \hat{\boldsymbol{t}}, \hat{\boldsymbol{\theta}}\}$, (see figure 1) and write the boundary conditions given by (2.13), above, in a more convenient form. Components of vectors and tensors in these directions will be denoted by the appropriate subscripts: n, t or θ. Arc-length and normal derivatives are written $\partial/\partial s$ and $\partial/\partial n$ respectively. The cylindrical radial coordinate and unit vector are denoted by r and $\hat{\boldsymbol{r}}$, with z measured from the free surface in the vertical direction.

The quantity $\nabla_s\cdot(\mu_s\boldsymbol{E}_s) = \mu_s\nabla_s\cdot\boldsymbol{E}_s + (\partial\mu_s/\partial s)\hat{\boldsymbol{t}}\cdot\boldsymbol{E}_s$ which appears when (2.14) is substituted into (2.13) can be evaluated by first recognising that $\boldsymbol{E}_s = \hat{\boldsymbol{t}}\hat{\boldsymbol{t}}e_{tt} + \hat{\boldsymbol{\theta}}\hat{\boldsymbol{\theta}}e_{\theta\theta}$, where $e_{tt} = \hat{\boldsymbol{t}}\cdot\nabla\boldsymbol{v}\cdot\hat{\boldsymbol{t}}$ and $e_{\theta\theta} = \hat{\boldsymbol{\theta}}\cdot\nabla\boldsymbol{v}\cdot\hat{\boldsymbol{\theta}}$, so that

$$\nabla_s\cdot\boldsymbol{E}_s = \left[\frac{\partial e_{tt}}{\partial s} + (e_{\theta\theta} - e_{tt})\tilde{\kappa}^{(\theta)}\right]\hat{\boldsymbol{t}} + \left[e_{tt}\kappa^{(t)} + e_{\theta\theta}\kappa^{(\theta)}\right]\hat{\boldsymbol{n}}. \tag{2.15}$$

In the above expression,

$$\kappa^{(t)} \equiv -\hat{\boldsymbol{t}}\cdot\nabla\hat{\boldsymbol{n}}\cdot\hat{\boldsymbol{t}}, \quad \kappa^{(\theta)} \equiv -\hat{\boldsymbol{\theta}}\cdot\nabla\hat{\boldsymbol{n}}\cdot\hat{\boldsymbol{\theta}} \equiv -\frac{\hat{\boldsymbol{n}}\cdot\hat{\boldsymbol{r}}}{r} \quad \text{and} \quad \tilde{\kappa}^{(\theta)} \equiv -\frac{\hat{\boldsymbol{t}}\cdot\hat{\boldsymbol{r}}}{r}, \tag{2.16}$$

with the total surface curvature defined as $\kappa = -\nabla_s\cdot\hat{\boldsymbol{n}} = \kappa^{(t)} + \kappa^{(\theta)}$.

We also require the quantity $\nabla_s\cdot(\mu_s\boldsymbol{D}_s) = \mu_s\nabla_s\cdot\boldsymbol{D}_s + (\partial\mu_s/\partial s)\hat{\boldsymbol{t}}\cdot\boldsymbol{D}_s$, together with a similar term involving the dilatational viscosity coefficient. Writing $\Delta = \nabla_s\cdot\boldsymbol{v}$(=

$e_{tt} + e_{\theta\theta}$) and using the definition of the surface identity in the first equation of (2.9), we see that

$$\nabla_s \cdot (\boldsymbol{I}_s \Delta) = \boldsymbol{I}_s \cdot \nabla_s \Delta - (\nabla_s \cdot (\hat{\boldsymbol{n}}\hat{\boldsymbol{n}}))\Delta$$

$$= \frac{\partial \Delta}{\partial s}\hat{\boldsymbol{t}} + \kappa \hat{\boldsymbol{n}}\Delta. \tag{2.17}$$

Likewise, we have

$$\nabla_s \cdot (\boldsymbol{I}_s \sigma) = \frac{\partial \sigma}{\partial s}\hat{\boldsymbol{t}} + \kappa \hat{\boldsymbol{n}}\sigma. \tag{2.18}$$

Finally, putting together (2.14), (2.15), (2.17) and (2.18) and using the identity

$$\frac{\partial e_{\theta\theta}}{\partial s} = \tilde{\kappa}^{(\theta)}(e_{\theta\theta} - e_{tt}) - \kappa^{(\theta)}\hat{\boldsymbol{t}} \cdot \nabla \boldsymbol{v} \cdot \hat{\boldsymbol{n}}, \tag{2.19}$$

we find that the normal component of (2.13) is

$$-p_{gas} = -q - \frac{2}{We}\sigma\kappa + \frac{4}{Re}\left(e_{nn} - \beta_s \mu_s (\kappa^{(t)} - \kappa^{(\theta)})(e_{tt} - e_{\theta\theta}) - \beta_d \kappa_s (\kappa^{(t)} + \kappa^{(\theta)})(e_{tt} + e_{\theta\theta})\right). \tag{2.20}$$

and that the corresponding tangential component is

$$0 = -\frac{2}{We}\frac{\partial \sigma}{\partial s} + \frac{4}{Re}\left(e_{tn} - \beta_s \mu_s \left\{\frac{\partial}{\partial s}(e_{tt}) - \tilde{\kappa}^{(\theta)}(e_{tt} - e_{\theta\theta}) + \kappa^{(\theta)}\hat{\boldsymbol{t}} \cdot \nabla \boldsymbol{v} \cdot \hat{\boldsymbol{n}}\right\}\right.$$
$$-\beta_d \kappa_s \left\{\frac{\partial}{\partial s}(e_{tt}) - \tilde{\kappa}^{(\theta)}(e_{tt} - e_{\theta\theta}) - \kappa^{(\theta)}\hat{\boldsymbol{t}} \cdot \nabla \boldsymbol{v} \cdot \hat{\boldsymbol{n}}\right\}$$
$$\left. -\beta_s \frac{\partial \mu_s}{\partial s}(e_{tt} - e_{\theta\theta}) - \beta_d \frac{\partial \kappa_s}{\partial s}(e_{tt} + e_{\theta\theta})\right). \tag{2.21}$$

In (2.20) and (2.21), $e_{nn} = \hat{\boldsymbol{n}} \cdot \nabla \boldsymbol{v} \cdot \hat{\boldsymbol{n}}$ and $e_{tn} = \frac{1}{2}(\hat{\boldsymbol{t}} \cdot \nabla \boldsymbol{v} \cdot \hat{\boldsymbol{n}} + \hat{\boldsymbol{n}} \cdot \nabla \boldsymbol{v} \cdot \hat{\boldsymbol{t}})$.

3. Background to the boundary integral approach

In this section we describe briefly the boundary integral method that forms the backbone of the numerical technique described in §5. For more details on axisymmetric boundary integral methods applied to high Reynolds number flows, the reader should refer to Guerri *et al.* (1981), Taib (1985), or Blake, Taib & Doherty (1986, 1987).

The geometry for the problem is depicted in figure 1. On the free surface, $\mathscr{S}$, there is a surfactant surface concentration Γ; in the fluid, $\mathscr{D}$, there is a bulk concentration C. For the purposes of the numerical method, normals are taken as pointing towards the gaseous phase where the pressure, p_{gas}, is taken as constant atmospheric pressure.

Away from the boundary, the fluid flow is assumed irrotational. Together with the incompressibility assumption, this leads to the field equation being expressible as Laplace's equation,

$$\nabla^2 \phi = 0, \tag{3.1}$$

with the irrotational part of the velocity field given by $\boldsymbol{u} = \nabla\phi$.

The Green's formula approach is used to formulate Laplace's equation as a bound-

ary integral problem. This involves using the integral equation

$$\tfrac{1}{2}\phi(\boldsymbol{x}) = \int\!\!\!\!\!\!-_{\mathscr{S}} \left(G\frac{\partial \phi}{\partial n}(\boldsymbol{x}') - \phi(\boldsymbol{x}')\frac{\partial G}{\partial n'} \right) \mathrm{d}S', \tag{3.2}$$

where $\boldsymbol{x} \in \mathscr{S}$ and the Green's function is given by

$$G(\boldsymbol{x}, \boldsymbol{x}') = \frac{1}{4\pi}\frac{1}{|\boldsymbol{x} - \boldsymbol{x}'|}. \tag{3.3}$$

Numerical solution of (3.2) allows the normal velocity ($\partial\phi/\partial n$) to be found and hence the bubble surface shape updated at each time step. In the absence of viscous effects, the pressure balance at the surface can be used in conjunction with the Bernoulli theorem, written in terms of a material derivative, to provide a means for updating the surface potential. This evolution equation is simply

$$\frac{\mathrm{D}\phi}{\mathrm{D}t} = \tfrac{1}{2}|\boldsymbol{u}|^2 - \frac{Eo}{2We}z + \frac{2}{We}\sigma\kappa. \tag{3.4}$$

If bulk and surface viscous forces are present, although the change in the normal velocities is apparently small (see §4, below), the perturbation to the tangential velocity is coupled to the inviscid surface motion through the Lagrangian time derivative term of (3.4) which, in addition, will include terms due to the altered normal stress balance, allowing the possibility of significant variation in the resulting surface motion.

4. Boundary-layer approximation

In order to take account of the additional boundary condition represented by the tangential stress balance, (2.21), we need to include an additional tangential velocity as a perturbation to the inviscid velocity field which is found as a solution to the boundary integral equation (3.2). Nadim, *et al.* (1993) developed one technique for doing this. Their approach was to ignore the bulk viscous stress terms and solve the tangential stress condition for the total tangential velocity at each time step. However this method assumes that the viscous stresses in the boundary layer are less than any surface tension and surface viscous forces. As the boundary-layer thickness is of order $Re^{-1/2}$ (see below), surface viscous forces dominate bulk viscous forces in the tangential stress condition, (2.21), when either β_d or $\beta_s \gg Re^{1/2}$. So the Nadim *et al.* method does not allow us to examine the case where only moderate surface viscous effects are present. In addition to this we might expect the flow on certain parts of the surface, namely far from the axis of symmetry, to be dominated by bulk viscous stresses. Indeed, for large r the following order-of-magnitude estimates can be derived for the inviscid part of the flow (which will drive any boundary-layer perturbation) $u_t = O(r^{-4})$, $u_n = O(r^{-3})$ and $\kappa^{(t)}$, $\kappa^{(\theta)} = O(r^{-5})$ so $\hat{\boldsymbol{t}}\cdot\nabla\boldsymbol{u}\cdot\hat{\boldsymbol{t}}$, $\hat{\boldsymbol{n}}\cdot\nabla\boldsymbol{u}\cdot\hat{\boldsymbol{n}}$ and $\hat{\boldsymbol{\theta}}\cdot\nabla\boldsymbol{u}\cdot\hat{\boldsymbol{\theta}}$ are $O(r^{-5})$ whereas $\hat{\boldsymbol{t}}\cdot\nabla\boldsymbol{u}\cdot\hat{\boldsymbol{n}} = \hat{\boldsymbol{n}}\cdot\nabla\boldsymbol{u}\cdot\hat{\boldsymbol{t}} = O(r^{-4})$ as $r \to \infty$ (see BSB). In the normal stress condition, (2.20), the components of the surface rate-of-strain tensor are of equal order for all r so that the bulk stress term will be important for large Reynolds numbers only when the β_d and β_s are $O(1)$. However, the bulk viscous stress terms in the tangential condition, (2.21), will eventually dominate the surface viscous stresses for sufficiently large r, regardless of the values of β_s and β_d. Moreover, the method described is liable to break down if the balance with bulk viscous stresses is removed – the velocities produced when solving for the tangential velocity perturbation are found to *increase* as r approaches R_{max}, the outward extent of the computational domain.

To proceed, we write the velocity field (Lundgren & Mansour 1988; BSB) as

$$\boldsymbol{v} = \boldsymbol{u} + \boldsymbol{U}, \tag{4.1}$$

where $\boldsymbol{u} = \nabla\phi$ is the irrotational part and $\boldsymbol{U}$ is a perturbation due to a boundary layer. Similarly, we decompose the pressure, q, as

$$q = p + P, \tag{4.2}$$

where p is the liquid pressure due to the irrotational flow and P is a perturbation. For uniqueness, we insist that all perturbations tend to zero as the edge of the boundary layer is approached. To leading order we need to find only U_t and $\boldsymbol{u}$ as, in the thin boundary layer of thickness δ, $U_n \ll U_t$ and $P \ll p$; however in some cases a knowledge of U_n and P is also required (see below).

On using (4.1) and the fact that $\nabla\boldsymbol{u}$ is symmetric, we can write the tangential surface stress condition, (2.21), in a more convenient form,

$$\begin{aligned}\frac{\partial U_t}{\partial n} = {} & \frac{Re}{We}\frac{\partial \sigma}{\partial s} - (\hat{\boldsymbol{t}}\cdot\nabla\boldsymbol{v}\cdot\hat{\boldsymbol{n}} + \hat{\boldsymbol{t}}\cdot\nabla\boldsymbol{u}\cdot\hat{\boldsymbol{n}}) \\ & + 2\beta_s\mu_s\left\{\frac{\partial}{\partial s}(e_{tt}) - \tilde{\kappa}^{(\theta)}(e_{tt} - e_{\theta\theta}) + \kappa^{(\theta)}\hat{\boldsymbol{t}}\cdot\nabla\boldsymbol{v}\cdot\hat{\boldsymbol{n}}\right\} \\ & + 2\beta_d\kappa_s\left\{\frac{\partial}{\partial s}(e_{tt}) - \tilde{\kappa}^{(\theta)}(e_{tt} - e_{\theta\theta}) - \kappa^{(\theta)}\hat{\boldsymbol{t}}\cdot\nabla\boldsymbol{v}\cdot\hat{\boldsymbol{n}}\right\} \\ & + 2\beta_s\frac{\partial\mu_s}{\partial s}(e_{tt} - e_{\theta\theta}) + 2\beta_d\frac{\partial\kappa_s}{\partial s}(e_{tt} + e_{\theta\theta}).\end{aligned} \tag{4.3}$$

The boundary-layer equations can be derived using the surface-fitted coordinate system indicated above. We assume that the perturbation to the tangential velocity at the surface is, at most, of the same order as that of the irrotational component so that $U_t = O(1)$. The continuity equation implies that $\partial U_n/\partial n = O(1)$ and so, since $U_n \to 0$ as the edge of the boundary layer is approached, we must have $U_n = O(\delta)$. Likewise, as U_t falls from $O(1)$ to 0 in the layer, we assume $\partial U_t/\partial n = O(1/\delta)$.

At this point we should mention that in reality, owing to the translational component present in the potential flow, a thin rotational wake can be expected to start to form beneath the bubble as it collapses and rises. Indeed, in the calculations of BSB a region of separated flow is apparent during the burst, immediately prior to jet formation. This being the case, a boundary integral method of the kind described here cannot completely solve the problem as would other, more computationally expensive, finite-element or finite-difference approaches, but it can be used to offer valuable insight into the effects of surface contaminants on free-surface flows such as occur during bubble burst. In the light of this, no attempt has been made to try to resolve the higher tangential derivatives of the tangential velocity which may eventually develop near to the axis of symmetry as a result of a greater boundary-layer thickness there (Moore 1963). This would result in higher normal derivatives of the normal velocity and hence promote rapid movement of boundary-layer nodes away from the boundary (see §5 and (5.4), below).

Provided that the surface coordinates are taken with respect to the solution to the full boundary-layer equations, we can subtract the Euler equation, satisfied by the irrotational part of the flow, from the Navier–Stokes equations for the complete flow.

This gives a tangential equation (retaining only the largest viscous terms),

$$\frac{\mathrm{D}U_t}{\mathrm{D}t} + \boldsymbol{U}\cdot\nabla\boldsymbol{u}\cdot\hat{\boldsymbol{t}} - \boldsymbol{U}\cdot\frac{\mathrm{D}\hat{\boldsymbol{t}}}{\mathrm{D}t} = -\frac{\partial P}{\partial s} + 2Re^{-1}\frac{\partial^2 U_t}{\partial n^2}. \tag{4.4}$$

The $\mathrm{D}\hat{\boldsymbol{t}}/\mathrm{D}t$ term in (4.4) can be calculated using the fact that the interface of the bubble is a material surface so that $\hat{\boldsymbol{t}}$ points in the direction of the tangent to a material element. Its rate of change thus has a term $\hat{\boldsymbol{t}}\cdot\nabla\boldsymbol{v}$. Subtracting the $\hat{\boldsymbol{t}}$ component of this further ensures that $\hat{\boldsymbol{t}}$ remains a unit vector. Thus we find that

$$\frac{\mathrm{D}\hat{\boldsymbol{t}}}{\mathrm{D}t} = \hat{\boldsymbol{t}}\cdot\nabla\boldsymbol{v} - \hat{\boldsymbol{t}}(\hat{\boldsymbol{t}}\cdot\nabla\boldsymbol{v}\cdot\hat{\boldsymbol{t}}). \tag{4.5}$$

For an axisymmetric geometry, $\mathrm{D}\hat{\boldsymbol{t}}/\mathrm{D}t$ is entirely in the normal direction and so we can write

$$\frac{\mathrm{D}\hat{\boldsymbol{t}}}{\mathrm{D}t} = (\hat{\boldsymbol{t}}\cdot\nabla\boldsymbol{v}\cdot\hat{\boldsymbol{n}})\hat{\boldsymbol{n}}. \tag{4.6}$$

In the boundary-layer equation, (4.4), this will be multiplied by an $O(\delta)$ U_n term and so can be ignored.

The normal component of the boundary-layer equation is

$$\frac{\mathrm{D}U_n}{\mathrm{D}t} + \boldsymbol{U}\cdot\nabla\boldsymbol{u}\cdot\hat{\boldsymbol{n}} - \boldsymbol{U}\cdot\frac{\mathrm{D}\hat{\boldsymbol{n}}}{\mathrm{D}t} = -\frac{\partial P}{\partial n} + 2Re^{-1}\frac{\partial^2 U_n}{\partial n^2}. \tag{4.7}$$

The $\mathrm{D}\hat{\boldsymbol{n}}/\mathrm{D}t$ term in (4.7) cannot be calculated as above, as the normal is not related directly to a material element but follows the tangent, lagging by 90°. (Alternatively it can be derived by considering the rate of change of a unit element which rotates with the fluid but where changes due to straining motions are simply opposite to the corresponding changes for material elements.) Thus, using the fact that $\hat{\boldsymbol{t}}\cdot(\mathrm{D}\hat{\boldsymbol{n}}/\mathrm{D}t) = -\hat{\boldsymbol{n}}\cdot(\mathrm{D}\hat{\boldsymbol{t}}/\mathrm{D}t)$, we find

$$\frac{\mathrm{D}\hat{\boldsymbol{n}}}{\mathrm{D}t} = -\hat{\boldsymbol{n}}\cdot(\nabla\boldsymbol{v})^T + \hat{\boldsymbol{n}}(\hat{\boldsymbol{n}}\cdot\nabla\boldsymbol{v}\cdot\hat{\boldsymbol{n}}). \tag{4.8}$$

Again, for an axisymmetric geometry, this has only a tangential component and so

$$\frac{\mathrm{D}\hat{\boldsymbol{n}}}{\mathrm{D}t} = -(\hat{\boldsymbol{t}}\cdot\nabla\boldsymbol{v}\cdot\hat{\boldsymbol{n}})\hat{\boldsymbol{t}}. \tag{4.9}$$

If the normal velocity perturbation is to remain of $O(\delta)$ after unit time, the $\mathrm{D}U_n/\mathrm{D}t$ term in the normal boundary-layer equation, (4.7), must be $O(\delta)$ even though a convection term contributing to this rate of change is $O(1)$ (Lundgren & Mansour 1988). This is the same as assuming that the boundary-layer thickness remains $O(\delta)$ so that the $O(1)$ time variation at a fixed point in the fluid is due to the surface, and hence boundary layer, moving away from the point, through the $O(1)$ normal derivative of U_n, with an $O(1)$ speed, u_n.

Using the tangential component of the boundary-layer equations, (4.4), we see that the pressure perturbation must fall to zero outside the boundary layer. The remaining terms of the normal boundary-layer equation, (4.7), thus imply that $\partial P/\partial n = O(1)$ so that $P = O(\delta)$ in the boundary layer.

We can thus ignore $\partial P/\partial s$ in the tangential boundary-layer equation, (4.4). Further, a balance of viscous and inertia forces in (4.4) gives us the result that $\delta = O(Re^{-1/2})$.

Taking the above arguments into account, the normal boundary-layer equation becomes

$$U_t\left(2\frac{\partial u_n}{\partial s}+\kappa^{(t)}(2u_t+U_t)\right)=-\frac{\partial P}{\partial n}. \tag{4.10}$$

To see when the pressure perturbation will be important, we consider different cases where β_d and β_s are of varying orders of magnitude, the greatest of which, for brevity, we denote β. Provided that we ignore effects of surface tension gradients, the tangential stress condition, (4.3), tells us that U_t, at least for $\beta = O(\delta^{-1})$, is of order $\beta\delta$. For $\beta \gg \delta^{-1}$ we expect to approach the case of a tangentially rigid boundary, in which case the perturbation to the velocity must remain of the same order as the potential flow velocity which drives the flow and the subsequent generation of any rotational motion. In this latter case, the term on the left-hand side of (4.3) is small compared to the surface viscous terms, so that bulk viscous stresses can be ignored and, as in the numerical method of Nadim *et al.* (1993), the tangential velocity is determined by a balance of the surface viscous and surface tension gradient terms.

The first case that we consider is $\beta = O(1)$ so that $U_t = O(\delta)$, and we find ourselves in a situation similar to that of a stress-free interface. In this case both the bulk and surface viscous terms, as well as the pressure perturbation in the normal stress condition, (2.20), will be $O(\delta^2)$. This case is not particularly interesting for bursting bubbles as was seen in BSB, so we shall go on to examine the case $1 \ll \beta \ll \delta^{-1}$. Now, $\delta \ll U_t \ll 1$ and examination of the normal stress condition shows that the pressure perturbation and the surface viscous terms are of order $\beta\delta^2$, while the bulk viscous terms are only of order δ^2. Clearly, the pressure perturbation and surface viscous terms also match in cases when β is of order δ^{-1}. In the final case, we consider $\beta \gg \delta^{-1}$ with the assumption that U_t remains $O(1)$. In this case the surface viscous terms dominate all other terms in the normal stress condition. From this brief discussion we see that the pressure perturbation term in the normal stress condition is required in all cases except when one of β_d or β_s is much larger than δ^{-1}.

To solve for the bulk surfactant concentration in the case where the surfactant is soluble requires us to consider the corresponding concentration boundary layer. First we decompose the concentration into $C = 1 + C'$, so that $C' \to 0$ as the edge of the boundary layer is approached. The dimensionless form of (2.7) for the concentration perturbation, C', is

$$\frac{DC'}{Dt} = 2Pe^{-1}\nabla^2 C'. \tag{4.11}$$

As in the case of the equation for the tangential velocity, the left-hand side of (4.11) is of order C' owing to the cancellation of convective and time derivatives. If the concentration boundary-layer thickness is δ_c, then the right-hand side is of order $Pe^{-1}C'/\delta_c^2$. If the diffusive terms are to balance the convective terms, we must take $\delta_c = O(Sc^{-1/2}\delta)$. So if $Sc \gg 1$ the concentration boundary layer will be much smaller than the vorticity boundary layer. In order to allow the use of just one boundary-layer mesh (see below), we assume that $D^* = O(\nu^*)$. This is perhaps somewhat unrealistic, as for most surfactants $D^* \ll \nu^*$, nevertheless it serves to illustrate the potential of the method. In particular, in the examples given below we take $Pe = Re$, i.e. $Sc = 1$.

5. Solution scheme

In order to solve this problem numerically, we need to keep track of the positions of boundary-layer nodes used to form a mesh adjacent to the interface. This mesh

can then be employed to allow the calculation of normal and tangential derivatives in the layer. For the stress-free surface condition, applicable to a pure interface, material normals to the surface remain perpendicular and straight (to first order in δ) as the surface deforms (see BSB). In the case where surfactants are present, the surface tangential stress is non-zero but can easily be calculated. Thus it is still possible to move boundary-layer points so that they remain fixed on normals to the surface, free only to move up and down these normals (see figure 2). To do this we need to change the velocity with which points are advected from $\boldsymbol{v}$ to some $\boldsymbol{v}^*$ which is linear in the normal coordinate, η, and satisfies $\hat{\boldsymbol{n}} \cdot \boldsymbol{v} = \hat{\boldsymbol{n}} \cdot \boldsymbol{v}^*$ and zero tangential stress at the interface.

In order to find such a velocity, we first allow the tangential component of the velocity to vary, thus increasing accuracy and lessening the need for repositioning of surface nodes. That is we define $\boldsymbol{v}(\epsilon) = v_n\hat{\boldsymbol{n}} + \epsilon v_t\hat{\boldsymbol{t}}$, for some $\epsilon \in [0, 1]$. We now take the first two terms in the Taylor expansion of the velocity with respect to the normal coordinate, η, and subtract a vector in the tangential direction proportional to the size of the tangential component of the bulk stress tensor evaluated at the interface,

$$\boldsymbol{v}^*(\epsilon) = \boldsymbol{v}(\epsilon)|_0 - \eta(\hat{\boldsymbol{n}} \cdot \nabla \boldsymbol{v}(\epsilon))\Big|_0 + \eta\hat{\boldsymbol{t}}\,(\hat{\boldsymbol{t}} \cdot \nabla \boldsymbol{v}\,(\epsilon) \cdot \hat{\boldsymbol{n}} + \hat{\boldsymbol{n}} \cdot \nabla \boldsymbol{v}\,(\epsilon) \cdot \hat{\boldsymbol{t}})\Big|_0. \tag{5.1}$$

This simplifies to

$$\boldsymbol{v}^*(\epsilon) = \boldsymbol{v}(\epsilon)|_0 + \eta\left[(\hat{\boldsymbol{t}} \cdot \nabla \boldsymbol{v}\,(\epsilon) \cdot \hat{\boldsymbol{n}})\hat{\boldsymbol{t}} - (\hat{\boldsymbol{n}} \cdot \nabla \boldsymbol{v}\,(\epsilon) \cdot \hat{\boldsymbol{n}})\hat{\boldsymbol{n}}\right]\Big|_0, \tag{5.2}$$

where $|_0$ denotes evaluation at $\eta = 0$.

For brevity, we use a notation similar to that of BSB to represent time derivatives following particles moving with some velocity $\boldsymbol{w}$,

$$\frac{\mathrm{D}^{\boldsymbol{w}}}{\mathrm{D}t} \equiv \frac{\partial}{\partial t} + \boldsymbol{w} \cdot \nabla. \tag{5.3}$$

We now carefully replace the material derivatives in (2.6), (3.4), (4.4) and (4.11) with ones following particles that move with velocity $\boldsymbol{v}^*(\epsilon)$, to give us evolution equations for the surface concentration, the velocity potential, the perturbation to the tangential velocity and the bulk concentration perturbation respectively. For specific details regarding these equations, the reader is referred to the Appendix.

Having derived the equations of motion in terms of an advection velocity $\boldsymbol{v}^*(\epsilon)$, the heights of the boundary-layer nodes are governed by

$$\frac{\partial \eta}{\partial t} = -\hat{\boldsymbol{n}} \cdot \left(\boldsymbol{v}^*(\epsilon) - \boldsymbol{v}^*(\epsilon)|_0\right) = \eta \frac{\partial v_n}{\partial n}\Big|_0. \tag{5.4}$$

The form of (5.4) implies that all nodes along a normal will remain distributed in direct proportion to their initial spacing. Thus in computations we assume an initial constant spacing along each normal and store the position of only the outermost node.

To solve for the motion of the bubble, incorporating the boundary-layer flow induced by the presence of a surfactant, we need to couple, in some way, the Navier–Stokes boundary-layer approximation with the tangential stress condition. In order to do this, we utilize the technique used by Nadim *et al.* (1993). The Nadim *et al.* method does not include a boundary layer, as indicated above, and hence does not use any field equations other than the Laplace equation. Their approach is to calculate the tangential velocity perturbation directly from a tangential boundary stress condition, which takes a form similar to (4.3) with the absence of the bulk viscous terms. This

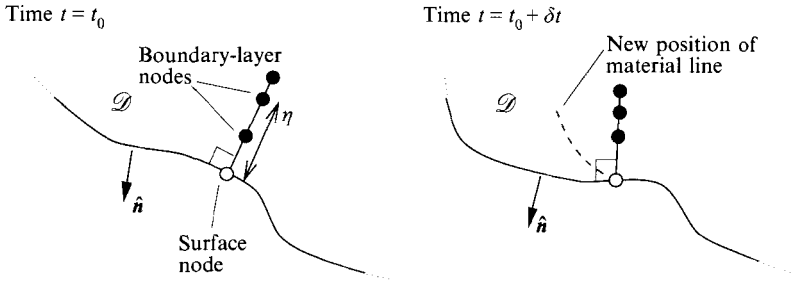

FIGURE 2. The boundary layer is discretized using nodes along normals to the surface. The nodes are kept fixed on the normals by utilizing a linearized material derivative.

is then used in the normal stress condition and the Bernoulli and boundary integral equations are solved implicitly for the updated potential and normal velocity.

The method that we employ here is as follows.

(*a*) At the beginning of each time step, the position of the surface and the potential and surface concentration at the surface are known. Also known are the values of the perturbations to the tangential velocity, U_t, and to the concentration, C', at nodes along normals to the surface, but *not* at the surface node where the normal meets the surface. In addition, the heights of the nodes on the normals are known.

(*b*) The boundary integral equations are solved for the normal velocity, $\partial\phi/\partial n$.

(*c*) The tangential balance, (4.3), is solved for the value of the perturbation to the tangential velocity, U_t, at the surface. This requires that the derivative $\partial U_t/\partial n$ be approximated using some finite-difference approach. In practice a low-order (e.g. quadratic) Lagrangian polynomial can be used interpolate the unknown U_t at the surface and a few of the known values of U_t along the normals at nodes adjacent to the surface.

The tangential derivatives at the surface are approximated using a cubic spline. Natural boundary conditions, i.e. $\partial^2 U_t/\partial s^2 = 0$, are used for the spline at the axis of symmetry. For the case of a free surface, the boundary condition on the spline at the outermost reach, $r = R_{max}$ (typically 20), is to clamp $\partial U_t/\partial s$ based on the assumption that for large r, $U_t(r) = U_t^{max}(R_{max}/r)^4$, where U_t^{max} is the value of U_t at $r = R_{max}$. The resulting equations are linear.

(*d*) The surface values of the bulk concentration are found by applying a (quadratic) finite difference scheme to the two equations for the flux, (2.10) and (2.11). Unlike in (*b*), above, there are no arc-length derivatives in this equation so that the values of $C'|_0$ at each of the nodes can be found separately.

(*e*) Now that U_t and C' are known throughout the boundary layer, the unsteady boundary-layer equations written in terms of the advection velocity $\boldsymbol{v}^*(\epsilon)$ – see (A 1) and (A 3) – can be used to find the changes in U_t and C' everywhere except at the surface. At the same time (A 2) is used to find the updates for the potential. Equation (5.4) is used to find the updates for the positions of the nodes along the normals.

The perturbation to the pressure, P, in the dynamic boundary condition for the potential given by (A 2), is found by numerically integrating the normal boundary-layer equation, (4.10), from outside the boundary, where P is assumed zero, towards the surface.

(*f*) The tangential velocity perturbation, bulk and surface concentrations, surface potential, surface position, and boundary-layer node positions are updated using a time-stepping rule.

6. Results and discussion

In this section we examine the results of the computational method developed in the previous sections to ascertain some of the effects that surfactants can have on the motion of a bursting bubble. The dependence of the bursting process upon the bubble size has been dealt with in detail, both experimentally (Newitt, Dombrowski & Knelman 1954; Garner, Ellis & Lacey 1954) and theoretically (BSB; Garcia-Briones & Chalmers 1993) on a number of previous occasions. We therefore concentrate our attention on one particular size of bubble ($Eo = 0.3$) and fix the bulk properties of the liquid ($M = 10^{-11}$ giving a Reynolds number of about 590), but allow the surface properties to vary.

In order to distinguish the separate phenomena caused by surface tension gradients and by the two types of surface viscosity considered, we select just one of these three properties to be in effect in any single calculation. Whilst this is clearly not physically realistic, it gives a flavour of some of the behaviour that might be expected. We also neglect the effect of surface diffusion in all calculations on the assumption that the surface diffusion coefficient is comparable to bulk diffusion so that its effect will be small during the lifetime of the burst.

We examine the effects that particular surface properties have on the evolution of the interfacial shape as a functions of time. Differences in the motion of the free surface between the case of a pure liquid and the case when surface forces are significant are of importance as they give us insight into the way in which the underlying fluid motion is altered through the changed surface stress condition.

From the above discussion in §4, we expect that it will be the tangential motion which is affected most by the presence of surfactants. We expect some properties, particularly surface dilatational viscosity, to have the effect of damping surface compression. We therefore anticipate the surface concentration on the interface, both spatially and temporally, to be highly dependent on the values of the various parameters governing the behaviour of the surfactant.

In BSB it was shown that large energy dissipation rates occur on the surface as a high-speed liquid jet is formed in the latter stages of the burst of a small bubble in a pure liquid. This work was motivated by the need to explain the observation of mammalian cell damage in sparged bioreactors in the presence of bursting bubbles. Cell death rates in this situation are observed to be greatly reduced by the addition of certain surfactants to the bioreactor medium. To ascertain whether surface viscous properties could bring about such a reduction in the damage caused by a bursting bubble, we too examine the maximum value of the viscous energy dissipation rate evaluated on the symmetry axis at the surface of the bubble as it bursts.

A recent report in the cell culture literature (Garcia-Briones & Chalmers 1994) indicates that in rotational flows the energy dissipation rate alone is not sufficient to characterize the damage potential of the flow field. Indeed it has been proposed that the difference between the rate of rotation of the principal axes of the rate-of-strain tensor and the local rotation speed of a fluid element forms an additional term in the equation for the determination of the damage potential. Since significant vorticity develops near to the boundary of a bursting bubble when there is a strong surfactant present, we expect the energy dissipation rate at the surface to be a poor indicator of possible cell damage. We therefore examine only the maximum energy dissipation rate achieved at the bubble surface on the axis of symmetry, where fluid rotation is zero, and leave a more detailed examination of the cell damage capability of the flow field for a future study.

For an incompressible fluid, the viscous energy dissipation rate evaluated at the surface and made non-dimensional with respect to $\rho^* U^{*2}/T^*$ can be written (to leading order in $Re^{-1/2}$) as

$$\Phi = \frac{2}{Re}\left\{4(e_{tt}^2 + e_{\theta\theta}^2 + e_{tt}e_{\theta\theta}) + \left(\hat{\boldsymbol{t}}\cdot\nabla\boldsymbol{v}\cdot\hat{\boldsymbol{n}} + \hat{\boldsymbol{t}}\cdot\nabla\boldsymbol{u}\cdot\hat{\boldsymbol{n}} + \frac{\partial U_t}{\partial n}\right)^2\right\}. \tag{6.1}$$

For a pure liquid or on the symmetry axis, the squared term in parentheses on the right of (6.1) can be taken to be zero owing to the vanishing tangential stress at the interface.

Some of the calculations described below break down before any jet can form. This is due to boundary-layer thickening (see also BSB) which, as well as violating the assumptions of the model, if restricted to a narrow region can cause arc-length derivatives in the boundary layer to become large (see (A 6)), leading to large rates of change of boundary-layer quantities such as the perturbation to the tangential velocity. When the size of the time step (chosen so as to ensure that the maximum changes in each of the variables ϕ, U_t, Γ and C' are bounded by some prescribed values) falls below some small number (10^{-5}, say), the calculation is stopped.

6.1. *The pure interface*

In figure 3(*a*), the motion of the interface for the bursting of a pure bubble is shown. It can be clearly seen from the figure that there is a surface wave which runs down the collapsing bubble crater, moving towards the symmetry axis. This wave emanates from the rapid retreat of the circular rim at the top of the bubble crater (the site of connection of the bubble to the thin liquid film which ruptured immediately prior to the commencement of the calculation). When the wave reaches the axis, a high-speed liquid jet is forced upwards.

We can quantify the compression of the surface during the burst if we plot the surface concentration of some dynamically inert material placed on the surface, as a function of arc-length for various times during the bursting process. This is done with the aid of (A 4) for the case $Pe_s = \infty$. Figure 4 shows the evolution of this surface concentration profile as the bubble bursts. A ring of high concentration forms as the wave mentioned above compresses the surface fluid as it passes along.

Well ahead of the surface concentration wave on figure 4(*a*, *b*), the concentration increases steadily as a result of the almost spherical collapse of the lower portion of the bubble surface (see figure 3*a*).

The concentration on the compression wave itself rises rapidly as it moves inward prior to jet formation. During jet rise, the surface concentration on the axis of symmetry exceeds its original value by a factor of almost 200 (see table 1, below). As the jet continues to rise, the local surface area will slowly increase again causing the surface concentration to fall slightly (see figure 7*b*, below) before a droplet is pinched off.

Just in front of the compression wave is a small area of expansion where, for figure 4(*a*–*c*), the surface concentration remains approximately equal to 1. Therefore, until the jet is about to form, the rate of expansion due to the surface wave almost balances the net compression resulting from the spherical collapse of the bubble crater. Immediately prior to jet formation, as the front of the surface wave reaches the symmetry axis, this is no longer the case and the surface expansion dominates for a short while, causing the surface concentration to drop below 1 in figure 4(*d*) (see also figure 7*b*).

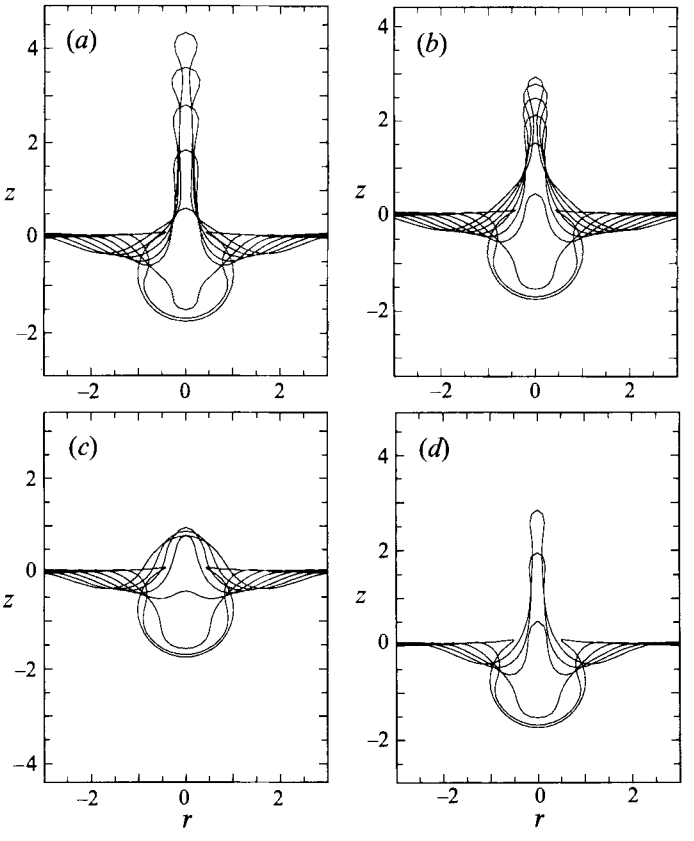

FIGURE 3. The surface shape evolution for a small bubble, with $Eo = 0.3$, for various surface properties: (*a*) pure, inviscid calculation, (*b*) low dilatational viscosity ($\beta_d = 10$), (*c*) moderate dilatational viscosity ($\beta_d = 50$), (*d*) surface tension gradients ($\alpha = 0.5$, $\Gamma_\infty = 12$, $\sigma_\infty = 0.1$) for an insoluble surfactant. In each case the time interval between frames is 0.2 and, for (*b*) onwards, the Morton number is 10^{-11}

Behind the surface wave is a second ring of low concentration due to the expansion of the surface corresponding to the radially outward motion of the rim of the bubble crater. As the rim widens, due to surface waves moving in both directions, so does the low-concentration ring. Owing to the overall flattening of the surface coupled to the surface compression near to the axis of symmetry, the arc-length position of the far end of the low-concentration ring does not alter much as time proceeds, even though reference to figure 3(*a*) shows a surface wave moving away from the symmetry axis.

6.2. *The effect of surfactants on the shape evolution*

Figure 3(*b–d*) shows the shapes of the free surface for bursting bubbles with various types of surface property.

We first examine the effect of surface dilatational viscosity which is depicted in figure 3(*b,c*). For the case of a low dilatational viscosity ($\beta_d = 10$, figure 3*b*) an examination of the early motion (particularly the second frame) indicates the surface wave seen in the pure case to be less clearly defined, indicating a damping effect. Jet formation itself requires a certain amount of surface expansion which is resisted by the dilatational viscosity. The jet resulting from the convergence of the wave on the

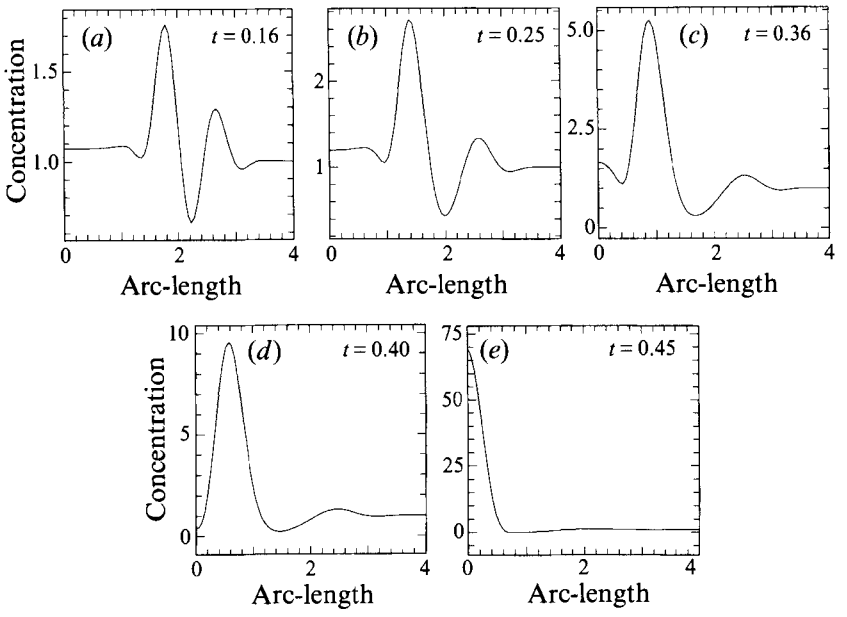

FIGURE 4. The evolution of surface concentration of an inert material as a function of arc-length for an otherwise pure bursting bubble.

axis of symmetry is thus initially slower than in the pure liquid case. The jet appears, however, to be narrower at its tip with the bulk of the rising fluid remaining in its much broader base.

The case when dilatational viscosity is moderately large ($\beta_d = 50$, figure 3*c*) is initially similar, with a slightly weaker surface wave. Later on, a jet starts to form although it is noticeably slower and the energy lost due to the surface dilation during its inception prevents a sharp jet tip from forming.

For the case of surface shear viscosity, there is very little difference in the early motion as compared with the pure case, except that the surface wave is damped slightly. Unfortunately the calculation breaks down before any jet can be formed. The method fails for this case – where it succeeded for the dilatational viscosity case, for example – since, according to (5.4), the boundary-layer thickness increases at a rate proportional to $\partial v_n/\partial n|_0$. Conservation of mass implies that this rate is just $-\nabla_s \cdot \boldsymbol{v}$, a term which appears on the right-hand side of the surface transport equation, (A 4). We shall see later (§6.3) that surface dilatational viscosity and the presence of surface tension gradients inhibit surface compression and so in these cases the method can continue past jet formation. Surface shear viscosity alone does not prevent significant surface compression thus resulting in boundary-layer thickening.

We consider two cases where surface tension is assumed to be a function of the surface concentration of surfactant: when the surfactant is considered insoluble and when it is considered soluble. For the case where the surfactant is insoluble, we expect the surface pressure to increase near the bottom of the bubble thus creating a resistance to further surface compression. The surface motion for the case where $\sigma_\infty = 0.1$, $\Gamma_\infty = 12$ and $\alpha = 0.5$ is shown in figure 3(*d*). Owing to the surfactant's effect on the surface tension, the initial configuration is slightly different from that shown previously in figure 3(*a–c*). In itself this makes very little difference to the subsequent motion (see BSB), although the changed surface tension alters very slightly the timescale over which the burst occurs.

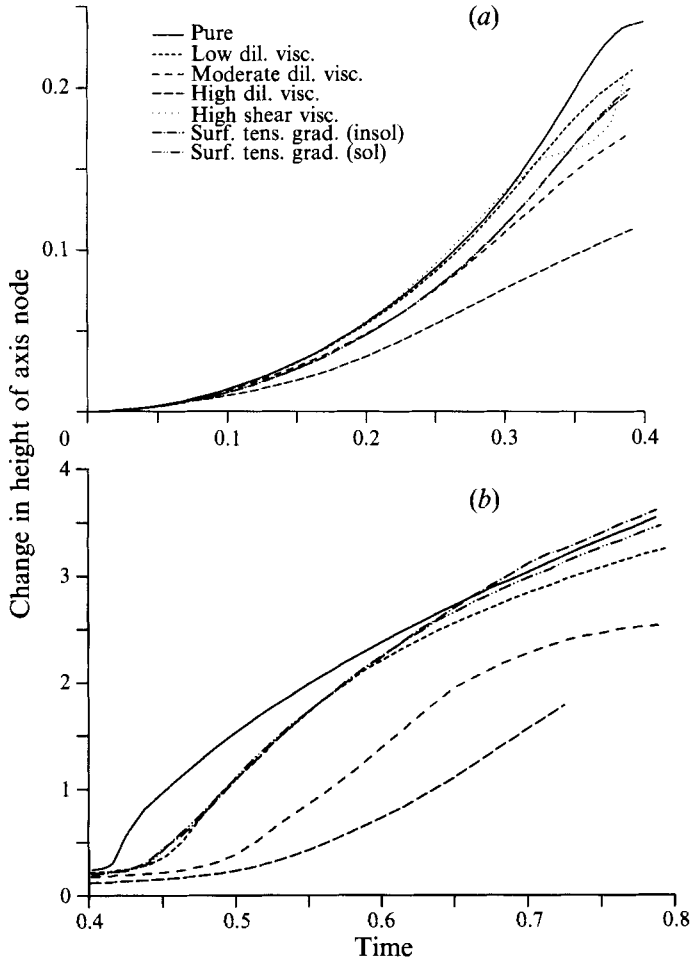

FIGURE 5. The change in height of the node on the symmetry axis during (*a*) the early motion and (*b*) jet formation of a bursting bubble plotted as a function of time for various cases. (For a quantitative description of the terms used see table 1.)

For insoluble surfactants the evolution of surface shape appears to be similar to that in the case of a low dilatational viscosity. The inward-moving capillary wave is again damped, but the jet is narrower and so faster. There is very little difference apparent between cases when the surfactant is soluble (with $h = 0.1$, $K = 10$) and when it is insoluble, so we plot only the insoluble case.

In order to see more clearly the effects of these surface properties, figures 5(*a*) and 5(*b*) show the change in height of the node on the axis of symmetry for various cases, during the early motion and subsequent jet formation respectively.

It it clear from figure 5(*a*) that the effect of dilatational viscosity is to retard the upward motion of the underside of the bubble. This can be explained by reference to figure 3. In all cases, it seems as though the lower portion of the bubble crater remains spherical and relatively undisturbed until the surface wave reaches it. We can therefore think of the early motion in terms of the isotropic collapse of a spherical cavity under the action of surface tension, for the case where the pressure inside is constant and equal to that of the far field. In order to model the early bubble burst

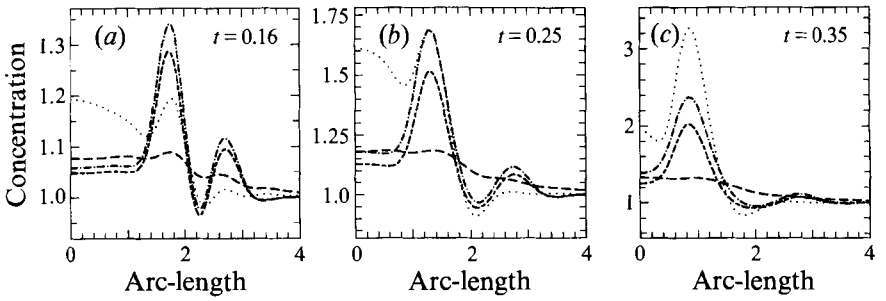

FIGURE 6. The evolution of surface concentration as a function of arc-length for contaminated bursting bubbles (— — —, $\beta_d = 50$; ····, $\beta_s = 50$; —· — ·—, $\alpha = 0.5$, $\Gamma_\infty = 12$, $\sigma_\infty = 0.1$, insoluble; – – –, $\alpha = 0.5$, $\Gamma_\infty = 12$, $\sigma_\infty = 0.1$, soluble ($h = 0.1$, $K = 10$)).

in this way we would also need to consider the force of surface tension which pulls the bursting bubble upwards towards the flat part of the free surface.

For the case of low surface dilatational viscosity, where a strong jet forms, the initial rise of the jet is much less rapid than that of the jet in the pure bubble case. Jet formation also occurs later than for the pure liquid case. The fact that the jet occurs only when the inward-moving surface wave converges on the axis of symmetry is also a factor that delays the inception of the weak jets of the moderate and large dilatational viscosity cases. These cases, as shown in figure 5(*a*), exhibit slower spherical collapse thus both lessening the amplification of the surface wave and increasing the distance that it has to travel.

The effect of surface tension gradients is very similar to that of surface dilatational viscosity: surface collapse is slower and the initial jet formation is much less rapid than in the pure case. The jet formation is again slightly later which is partly due to the smaller surface tension and thus longer timescale as mentioned above. Since the jets are thinner they are accelerated to higher velocities than in the pure case. In both the insoluble and soluble cases surface tension slows the jet after a short time, but due to the slightly greater surface concentration and thus lower surface tension in the insoluble surfactant case, this deceleration takes place more slowly than in the soluble case which follows fairly closely the curve for low dilatational viscosity.

Since surface shear viscosity has no effect for spherically symmetric motions, the finding, shown in figure 5(*a*), that the depth of the bottom of the bubble is altered very little by even a high surface shear viscosity is not unexpected. Prior to the calculation breaking down, the rate of rise of the bubble base decreases and then increases sharply as a jet is about to form. This is similar to what happens for the case of a pure interface (see figure 5*a*, *b*) and is explained in BSB, but it occurs earlier.

6.3. *The effect of surfactants on the tangential surface motion*

Although surfactants have been shown to have some effect on the motion of the bulk fluid during a bubble burst, the greatest effect will be at the surface. For moderate and large surfactant strengths, the boundary layer will allow significant slip between the tangential velocity of the bulk fluid and the tangential velocity at the surface. This effect is thus largely unseen in previous figures.

To appreciate the changes that occur in the surface motion we examine the surface concentration for various cases and compare it to the surface concentration for the

burst of a pure bubble. Thus we hope to indicate the effect of surface viscosity and surface tension gradients in preventing surface compression.

Close comparison of figure 6 to figure 4 shows that the concentration ahead of the converging surface wave in the case where there is moderate dilatational viscosity is very slightly higher than in the pure case. This is verified by examination of figure 7, below, which indicates that this effect is more striking for low surface dilatational viscosity where the surface concentration exceeds that on the pure interface until jet formation. This apparent contradiction with the observation that the bubble crater itself is seen to collapse slower when there is dilatational viscosity can be explained by the fact that surface dilatational viscosity will act so as to diffuse the higher surface compression caused by the advancing surface wave itself. The damping of this compression is seen clearly in figure 6. The effect of increasing the surface dilatational viscosity so that bulk viscous forces are comparatively small is to create an almost rigid surface so that the resultant compression is very small throughout the surface. Nevertheless even for the high dilatational viscosity the concentration on the symmetry axis exceeds that of the pure case for a short time.

In problems where the free surface can be considered flat to leading order, such as in the case of linearized surface waves, the $\kappa^{(\theta)}$ curvature coefficient of (2.20) and (2.21) is zero. Thus shear and dilatational viscous terms are identical and their effects cannot be distinguished. However when there is a large azimuthal curvature, as is the case along much of the surface of a bursting bubble, surface shear viscosity plays a quite different role. For nearly cylindrical surfaces, where the radius of the cylinder is of order unity, the coefficient $\tilde{\kappa}^{(\theta)}$ will be very small whereas $\kappa^{(\theta)} = O(1)$. This means that the $\hat{\boldsymbol{t}}\cdot\nabla\boldsymbol{v}\cdot\hat{\boldsymbol{n}}$ term in (4.3) will determine the effect of surface shear viscosity. From (4.6), we see that the effect of surface shear viscosity in this case will be to act to prevent the change in direction of the tangent at a surface particle.

Surface shear viscosity also has a slight damping effect on the concentration wave but, as with dilatational viscosity, it increases the surface concentration near the symmetry axis during the early motion well above that of the pure case. This seems to be a result of the shear viscosity preventing to some extent surface particles from going through the region on the surface in front of the surface wave where the rate of change of the tangent direction is large. The result is that the surface particles are swept along ahead of the wave. Indeed, from figure 6, the concentration behind the wave is quite small in comparison to most other cases.

The effect of surface tension gradients due to variations in surface coverage through compression and dilation of the surface is to impart a certain amount of elasticity to the surface fluid. This is particularly true in the case of insoluble surfactants, where the only way to relax a compressed surface is through a corresponding surface dilation. When the surfactant is soluble, relaxation of increased surface concentrations on compressed regions is possible through fluxes of adsorbed material into the bulk fluid. In this case, gradients in surface tension will give rise to forces similar to those due to surface dilatational viscosity; the surface stress can be considered to be dependent on the rate at which a surface is compressed or dilated. Indeed, in many studies (Lucassen & van den Tempel 1972) the surface dilatational viscosity has been defined in these terms. However Avramidis & Jiang (1991) call this an 'apparent' as opposed to an 'intrinsic' dilatational viscosity, and point to the consequent difficulty in experimentally isolating the intrinsic value.

Comparison of figures 4 and 6 shows that in the case of surface tension gradients, although there is damping of the compression wave, it is less noticeable than for the dilatational viscosity. Figure 7(*a*) also indicates that the concentration on the axis

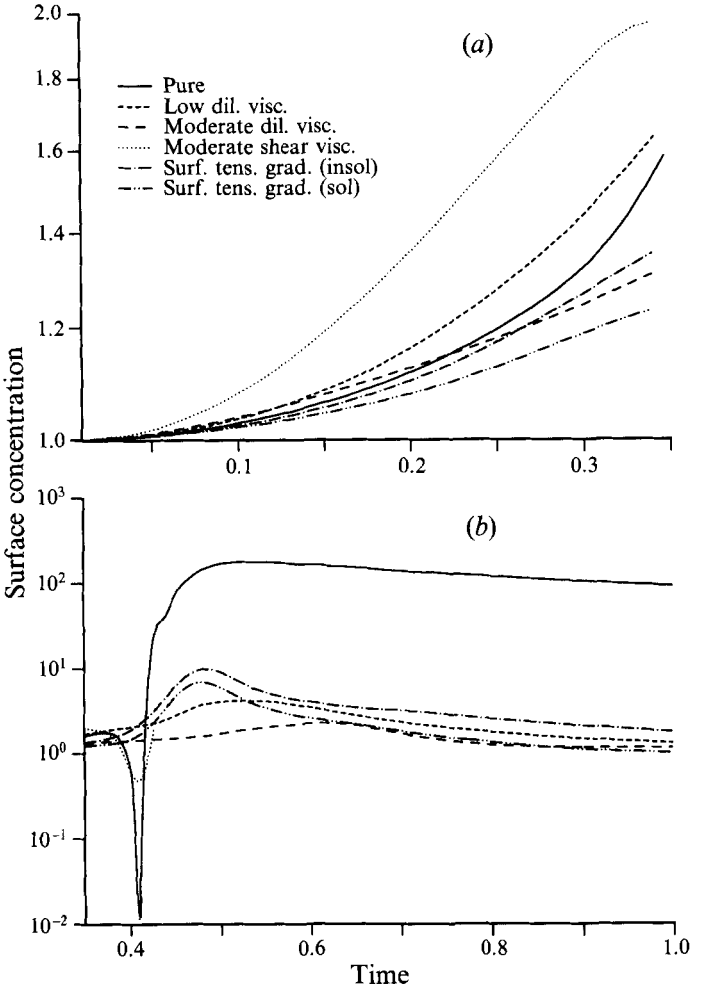

FIGURE 7. The surface concentration on the axis of symmetry as a function of time for (*a*) the early motion prior to jet formation and (*b*) the later motion during and after jet formation for various surface conditions. For a quantitative description of the terms see table 1.

remains below that of the pure case due to the fact that the compression wave, which occurs as a result of the surface elasticity imparted by the surface tension gradients, does not reach the axis until the jet is formed. However, the effect of the slight surface elasticity is seen in the gradual widening of the concentration wave in these cases in figure 6 as compared to figure 4. There is little difference between the cases of soluble and insoluble surfactants although in the soluble case the surface concentration is slightly lower.

An increase in surface concentration occurs at the axis of symmetry when a jet forms. From figure 7(*b*), we see that in two cases, pure liquid and moderate surface shear viscosity, the concentration increases quite suddenly as a jet forms, but before this increase there is a sharp decrease. This corresponds to the expansion region, which moves ahead of the wave of high concentration in these cases (figures 4 and 6), reaching the axis of symmetry. Owing to surface elasticity when surface tension gradients are included, the low concentration in front of the high-concentration wave

Surface property	Energy dissipation rate	Surface concentration
Pure liquid	390	180
Low surface dilatational viscosity ($\beta_d = 10$)	18	4.2
Moderate surface dilatational viscosity ($\beta_d = 50$)	19	2.3
High surface dilatational viscosity ($\beta_d = 300$)	15	1.3
Low surface shear viscosity ($\beta_s = 10$)	13	5.3
Moderate surface shear viscosity ($\beta_s = 50$)	22	5.4
High surface shear viscosity ($\beta_s = 300$)	280	5.1
Surface tension gradients ($\sigma_\infty = 0.1$, $\Gamma_\infty = 12$ and $\alpha = 0.5$)	98	11
As above with soluble surfactant ($K = 10$, $h = 0.1$)	96	7.3

TABLE 1. Maximum values of the dimensionless viscous energy dissipation rate evaluated at the intersection of the surface and the symmetry axis and dimensionless surface concentration for various surface properties. (In all runs, $Eo = 0.3$ and $M = 10^{-11}$.) In cases involving surface surface shear viscosity, the calculation breaks down before any jet can be produced.

vanishes before it reaches the axis, so that the fall in concentration is not observed. Here, as in the other cases plotted, the increase in surface concentration occurs steadily, over a longer timescale.

The effect of solubility is also clearly seen in figure 7. The surface concentration is slightly lower when surfactant desorption is included.

The maximum surface concentrations and surface energy dissipation rates occurring during the bursts are shown in table 1. This shows the maximum concentrations to be much lower in all cases involving dilatational viscosity and surface tension gradients. With dilatational viscosity, the energy dissipation rates are also smaller and this reflects the less violent flows occurring during jet production which we have seen in previous figures.

Note that for the particular parameters considered, the surface concentration for the insoluble surfactant where surface tension depends upon surface concentration comes close to the maximum value, Γ_∞, for which the surface equation of state, (2.12), is valid. There is no obvious way in which it can be decided *a priori* whether a calculation with a particular set of parameters will violate this condition. If it is found that Γ exceeds Γ_∞ during a calculation, then a more sophisticated equation of state is needed for such a case.

From table 1, the effect of surface shear viscosity is not entirely clear owing to the breakdown of the calculations as a jet is about to form. The many similarities between these calculations and that for the pure case, however, lead us to believe that the maximum values listed in the table may be significantly below what would have been obtained had the calculations run further.

Significant reductions in energy dissipation rates are also found in cases where surface tension gradients are considered. The maximum surface energy dissipation rates at the symmetry axis are approximately one quarter of that in the pure case. This is a real effect and is not just a consequence of the increased apparent timescale mentioned above. The initial surface tension changes by a factor of 0.86 with respect to the pure interface so that we would expect the rate of energy dissipation to decrease by a factor of just 0.93.

The effect of decreasing the adsorption depth, h, in problems where surfactant solubility is considered is to further increase the flux from the surface as the interface contracts. However, (see figure 8) each desorbed unit of surface material now

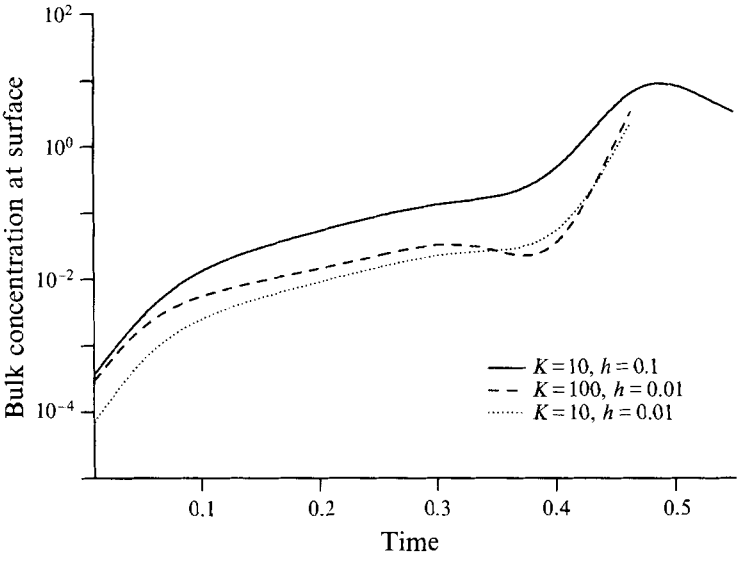

FIGURE 8. The bulk concentration evaluated at the surface on the axis of symmetry as a function of time for different values of the desorption rate, K, and adsorption depth, h.

corresponds to a lower bulk concentration when in solution; thus the rate of increase of bulk concentration is lower. From (2.10) and (2.11), the rate of increase of bulk concentration depends on the product Kh. Indeed calculations indicate that when Kh is kept constant, the bulk concentrations evaluated at the surface are asymptotic as $t \to 0$. For times much larger than the smaller value of K^{-1}, the bulk concentration for the more soluble case increases less rapidly than in the more soluble case.

7. Conclusions

We have developed a numerical technique, based on the boundary integral method, to allow the inclusion of a tangential surface stress condition through a boundary layer at high Reynolds numbers. We have applied this to the problem of a gas bubble bursting at a free surface in the presence of surfactants.

From the calculations made in just a few specific examples, we see that the surface motion, particularly during jet formation is highly dependent on surface properties. The surface concentration wave resulting from the inward-moving surface wave is, as expected, damped most significantly by surface dilatational viscosity, although also by surface elasticity. Unlike in the pure case, the rise in surface concentration is steady and slow. In addition, the formation of a high-speed liquid jet and the associated large energy dissipation rate during its formation can be prevented by a moderate surface dilatational viscosity. In the surface shear viscosity case, owing to the breakdown of the calculations prior to jet formation, there is little evidence of an effect on the surface shape evolution, but an increase in the surface concentration of surfactant near to the symmetry axis during the early motion is clearly apparent.

In relation to the mammalian cell damage problem mentioned briefly above, the significantly lower energy dissipation rates on the surface of a bursting bubble at the symmetry axis in many of the examples discussed indicate that those cells adhering to the bubble may not experience the large rates of strain during jet formation

which they would have done in a pure liquid. Although the precise properties of the surfactants used in practical bioreactor situations are not at present known, we can see from the calculations presented in this paper how they may result in a significant reduction in cell death rates as is observed in practice.

The author acknowledges the financial support given under the BBSRC grant No. GR/J57728. Gratitude is also due to Dr Ali Nadim and to Professor J.F. Harper for their useful advice. Finally, the author wishes to thank Mr Nick Emery, Dr Colin Thomas and the other members of the research group for invaluable discussions regarding this work, and especially Professor John Blake for taking the time to read and comment on this manuscript during its preparation.

Appendix. Evolution equations for the boundary layer

In this Appendix we derive explicit forms for the equations used to calculate rates of change of boundary-layer and surface quantities in terms of the operator $\mathrm{D}^{\boldsymbol{v}^\star(\epsilon)}/\mathrm{D}t$, which was introduced in §5.

From (4.4), the tangential perturbation velocity satisfies the following equation to leading order in δ:

$$\frac{\mathrm{D}^{\boldsymbol{v}^\star(\epsilon)}U_t}{\mathrm{D}t} = \left(\epsilon U_t|_0 - U_t + (\epsilon-1)u_t|_0\right)\frac{\partial U_t}{\partial s} + \left(U_n|_0 - U_n - \eta\frac{\partial U_n}{\partial n}\Big|_0\right)\frac{\partial U_t}{\partial n} + \left(u_n|_0\kappa^{(t)}|_0 - \frac{\partial u_t}{\partial s}\Big|_0\right)U_t + \frac{2}{Re}\frac{\partial^2 U_t}{\partial n^2}. \quad (A\,1)$$

It is important to point out that, even though we are not calculating U_n, (A 1) does give a good approximation to the rate of change of U_t. In neglecting U_n we lose a term $U_n\partial U_t/\partial n$ which can be of order 1 for large values of β_s and β_d. However, since we are also not including the perturbation to the normal velocity when we move the surface or boundary-layer nodes, (A 1) is correct, even though there is a small error in the surface motion.

For the dynamic condition, (3.4), used for updating the potential on the surface, we similarly find

$$\frac{\mathrm{D}^{\boldsymbol{v}^\star(\epsilon)|_0}\phi}{\mathrm{D}t} = \boldsymbol{u}\cdot\left(\boldsymbol{v}^\star(\epsilon) - \tfrac{1}{2}\boldsymbol{u}\right) - \frac{Eo}{2We}z + P + \frac{2}{We}\sigma\kappa - \frac{4}{Re}\left(e_{nn} - \beta_s\mu_s(\kappa^{(t)} - \kappa^{(\theta)})(e_{tt} - e_{\theta\theta}) - \beta_d\kappa_s(\kappa^{(t)} + \kappa^{(\theta)})(e_{tt} + e_{\theta\theta})\right), \quad (A\,2)$$

where $\boldsymbol{v}^\star(\epsilon)|_0$ is simply $u_n|_0\hat{\boldsymbol{n}} + \epsilon v_t|_0\hat{\boldsymbol{t}}$ to leading order in δ. The value of the pressure perturbation, P, at the surface can be calculated using the normal boundary-layer equation, (4.10).

The boundary-layer perturbation of the bulk concentration is updated using (4.11) which, in terms of the advection velocity $\boldsymbol{v}^\star$, becomes

$$\frac{\mathrm{D}^{\boldsymbol{v}^\star(\epsilon)}C'}{\mathrm{D}t} = \left(\epsilon U_t|_0 - U_t + (\epsilon-1)u_t|_0\right)\frac{\partial C'}{\partial s} + \left(U_n|_0 - U_n - \eta\frac{\partial U_n}{\partial n}\Big|_0\right)\frac{\partial C'}{\partial n} + \frac{2}{Pe}\frac{\partial^2 C'}{\partial n^2}. \quad (A\,3)$$

Likewise, the convection–diffusion equation for the surface concentration, (2.6), becomes

$$\frac{\mathrm{D}^{v^*(\epsilon)|_0}\Gamma}{\mathrm{D}t} = (\epsilon - 1)v_t|_0\frac{\partial \Gamma}{\partial s} - \Gamma\nabla_s\cdot\boldsymbol{v} + \frac{2}{Pe_s}\nabla_s^2\Gamma + j_n. \tag{A 4}$$

In order to determine the value of $\partial U_n/\partial n|_0$ in the equations for the evolution of U_t and C', (A 1) and (A 3), the continuity equation, which can be written in the form

$$\frac{\partial U_n}{\partial n} = -\frac{\partial U_t}{\partial s} + \tilde{\kappa}^{(\theta)}U_t + O(\delta), \tag{A 5}$$

is used. The appropriate limiting form is used on the axis of symmetry, namely replacing the right-hand side by $-2\partial U_t/\partial s + O(\delta)$. To find $U_n|_0 - U_n$, we utilize the fact that $\partial(U_n|_0 - U_n)/\partial n = -\partial U_n/\partial n$ and clearly $(U_n|_0 - U_n) = 0$ at $\eta = 0$, and integrate up through the boundary layer.

Care must be taken when calculating arc-length derivatives at points away from the boundary. This happens in (A 1) and (A 3) for U_t and C'. A cubic spline will allow interpolation of the values of U_t (say) at the jth node along each of the normals with respect to the surface arc-length. The error in the arc-length itself, resulting from the jth node being situated at a finite distance from the surface, is of order δ and so can be ignored. However the fact that $\partial U_t/\partial n = O(1/\delta)$ means that any small variations in the heights of the jth nodes in moving from one normal to the next are significant. Thus we write derivatives with respect to s, the arc-length parallel to the interface with η fixed (subject to the $O(\delta)$ error mentioned above), in terms of arc-length derivatives obtained by fitting a spline to the stored values of U_t along the 'material' line corresponding to fixed j,

$$\left.\frac{\partial U_t}{\partial s}\right|_{\text{fixed }\eta} = \left.\frac{\partial U_t}{\partial s}\right|_{\text{fixed }j} + \left.\frac{\partial U_t}{\partial n}\frac{\partial \eta}{\partial s}\right|_{\text{fixed }j}. \tag{A 6}$$

REFERENCES

ADAMSON, A. W. 1982 *Physical Chemistry of Surfaces.* Wiley-Interscience.

AVRAMIDIS, K. S. & JIANG, T. S. 1991 Measurement of the surface dilatational viscosity of aqueous gelatin–surfactant solutions. *J. Colloid Interface Sci.* **147**, 262–273.

BLAKE, J. R., TAIB, B. B. & DOHERTY, G. 1986 Transient cavities near boundaries. Part 1. Rigid boundary. *J. Fluid Mech.* **170**, 479–497.

BLAKE, J. R., TAIB, B. B. & DOHERTY, G. 1987 Transient cavities near boundaries. Part II. Free surface. *J. Fluid Mech.* **181**, 197–212.

BOULTON-STONE, J. M. & BLAKE, J. R. 1993 Gas bubbles bursting at a free surface. *J. Fluid Mech.* **254**, 437–466 (referred to herein as BSB).

GARCIA-BRIONES, M. A. & CHALMERS, J. J. 1993 Analysis of hydrodynamic information obtained from computer solutions of the rupture of a gas bubble in relation to animal cell damage in sparged bioreactors. In *Bioreactor and Bioprocess Fluid Dynamics* (ed. A. W. Nienow), pp. 191–210. Mechanical Engineering Publications.

GARCIA-BRIONES, M. A. & CHALMERS, J. J. 1994 Flow parameters associated with hydrodynamic cell injury. *Biotech. Bioengng* **44**, 1089–1098.

GARNER, F. H., ELLIS, S. R. M. & LACEY, J. A. 1954 The size distribution and entrainment of droplets. *Trans. Inst. Chem. Engrs* **32**, 222–235.

GAVER, D. P. & GROTBERG, J. B. 1990 The dynamics of a localized surfactant on a thin film. *J. Fluid Mech.* **213**, 127–148.

GUERRI, L., LUCCA, G. & PROSPERETTI, A. 1981 A numerical method for the dynamics of non-spherical cavitation bubbles. *Proc. 2nd Intl Colloq. on Drops and Bubbles, California*, pp. 175–181.

HARPER, J. F. 1972 The motion of bubbles and drops through liquids. *Adv. Appl. Mech.* **12**, 59–129.

HARPER, J. F. 1973 On bubbles with small immobile adsorbed films rising in liquids at low Reynolds numbers. *J. Fluid Mech.* **58**, 539–545.

HARPER, J. F. 1974 On spherical bubbles rising steadily in dilute surfactant solutions. *Q. J. Mech. Appl. Maths* **27**, 87–100.

HARPER, J. F. 1988 The rear stagnation region of a bubble rising steadily in a dilute surfactant solution. *Q. J. Mech. Appl. Maths* **41**, 203–213.

JENSEN, O. E. & GROTBERG, J. B. 1992 Insoluble surfactant spreading on a thin viscous film: shock evolution and film rupture. *J. Fluid Mech.* **240**, 259–288.

JENSEN, O.E. & GROTBERG, J. B. 1993 The spreading of heat or soluble surfactant along a thin liquid film. *Phys. Fluids* A **5**, 58–68.

JOHNSON, D. O. & STEBE, K. J. 1994 Oscillating bubble tensiometry: A method for measuring surfactant adsorptive–desorptive kinetics and surface dilatational viscosity. *J. Colloid Interface Sci.* **168**, 21–31.

LEMAIRE, C. & LANGEVIN, D. 1992 Longitudinal surface waves at liquid interfaces: Measurement of monolayer viscoelasticity. *Colloid Surf.* **65**, 101–112.

LEVICH, V. G. 1962 *Physicochemical Hydrodynamics.* Prentice-Hall, New Jersey.

LIN, S. Y., MCKEIGUE, K. & MALDARELLI, C. 1991 Diffusion-limited interpretation of the induction period in the relaxation in surface-tension due to the adsorption of straight chain, small polar group surfactants: Theory and experiment. *Langmuir* **7**, 1055–1066.

LUCASSEN, J. & TEMPEL, M. VAN DEN 1972 Longitudinal waves on visco-elastic surfaces. *J. Colloid Interface Sci.* **41**, 491–498.

LUNDGREN, T. S. & MANSOUR, N. N. 1988 Oscillations of drops in zero gravity with weak viscous effects. *J. Fluid Mech.* **194**, 479–510.

MOORE, D. W. 1963 The boundary layer on a spherical gas bubble. *J. Fluid Mech.* **16**, 161–176.

NADIM, A., KUMAR, S. & GREENSPAN, H. P. 1993 Boundary integral calculations of bubble dynamics in the presence of surfactants. Talk given at Am. Phys. Soc. Fluid Dynamics Division meeting, New Mexico.

NEWITT, D. M., DOMBROWSKI, N. & KNELMAN, F. H. 1954 Liquid entrainment 1. The mechanism of drop formation from gas or vapour bubbles. *Trans. Inst. Chem. Engrs* **32**, 244–261.

SADHAL, S. S. & JOHNSON, R. E. 1983 Stokes flow past bubbles and drops partially coated with thin films. Part 1. Stagnant cap of surfactant film — exact solution. *J. Fluid Mech.* **126**, 237–250.

SAVIC, P. 1953 Circulation and distortion of liquid drops falling though a viscous medium. *Nat. Res. Counc. Can., Div. Mech. Engng Rep.* MT–22.

SLATTERY, J. C. 1990 *Interfacial Transport phenomena.* Springer-Verlag, New York.

TAIB, B. B. 1985 Boundary element method applied to cavitation bubble dynamics. PhD thesis, University of Wollongong, Australia.